Biosensors and Bioelectronics 137 (2019) 1–7

Contents lists available at ScienceDirect

Biosensors and Bioelectronics

journal homepage: www.elsevier.com/locate/bios

Cascade catalysis-initiated radical polymerization amplified impedimetric immunosensor for ultrasensitive detection of carbohydrate antigen 15-3

Chi Zhang[1], Dongsheng Zhang[1], Zhanfang Ma[*], Hongliang Han[**]

Department of Chemistry, Capital Normal University, Beijing, 100048, China

ARTICLE INFO

Keywords:
Metal-organic frameworks
Cascade catalysis
Radical polymerization
Signal amplification
Impedimetric biosensor
Carbohydrate antigen 15-3

ABSTRACT

Efficient signal amplification strategies are crucial for ultrasensitive detection of tumor markers. Herein, a new signal amplification strategy by coupling cascade catalysis-initiated radical polymerization with impedimetric immunoassay was proposed for ultrasensitive detection of carbohydrate antigen 15–3 (CA15-3). Copper-based metal-organic framework nanoparticles (Cu-MOF), as peroxidase mimics, combined with CA15-3 antibody (Ab_2) and glucose oxidase (GOx) were employed as immunoprobes to initiate radical polymerization by cascade catalysis. In this work, the oxidation of glucose was catalyzed by GOx to generate hydrogen peroxide (H_2O_2), which reacted with acetylacetone (ACAC) via Cu-MOF catalysis to yield ACAC radicals for the polymerization of N-isopropylacrylamide (NIPAM). The polymer, poly (N-isopropylacrylamide) (PNIPAM), was generated in situ from the radical polymerization. As resistance enhancer, PNIPAM was covered on electrode surface to amplify resistance value by its poor conductivity. With the help of polymerization-based amplification, the resistance differences caused by target were improved significantly. Under optimum conditions, the designed biosensor showed wide detection ranges from 10 μU/mL to 10 mU/mL and 10 mU/mL to 100 U/mL, with ultralow detection limit of 5.06 μU/mL for CA15-3. Such an approach opened a new avenue for signal amplification, thus offering an ultrasensitive detection platform for a broad range of tumor markers.

1. Introduction

The ultrasensitive and high specific monitoring of tumor markers is the key to biomedical applications (Ren et al., 2017; Tang et al., 2017; Zhang et al., 2018b). According to reports, cancer is the leading cause of death in developed countries and the secondary cause in developing countries (Jemal et al., 2011). Of different types of cancer, breast cancer is the most common cancer among women globally (DeSantis et al., 2013; Marques et al., 2018). Carbohydrate antigen 15–3 (CA15-3), as one of the most reliable biomarkers of breast cancer, is below 30 U/mL in healthy human serum (de Oliveira et al., 2017; Li et al., 2013b). Also, CA15-3 concentration is related to the patients' post-operative status, recurrence rate and metastasis monitoring (Ke et al., 2018). Up to now, a series of analytical approaches have been proposed for CA15-3 detection, such as electrochemiluminescence (ECL) (Jiang et al., 2015; Zhang et al., 2015), radioimmunoassay (RIA) (Zhang et al., 2006), electrochemical immunoassay (EC) (Akbari Nakhjavani et al., 2018; Li et al., 2013a), and so forth. Specifically, electrochemical immunoassay has received a tremendous popularity due to its high specificity, rapid response and ease of miniaturization (Zhang et al., 2018a; Zheng et al., 2018).

As a valuable tool in electrochemical research (Sharma et al., 2018; Xie et al., 2018), electrochemical impedance spectroscopy (EIS) can detect the change of interfacial charge transfer resistance caused by fabrication process and recognition process on the electrode surface (Hashemi et al., 2017). Among electrochemical detection techniques, EIS technique is significantly sensitive for the detection of protein by its low dielectric constant and high molecular weight (Gao et al., 2018; Krittayavathananon and Sawangphruk, 2017; Park and Park, 2009; Xu et al., 2009). However, the detectable signal generated by the direct reaction between antigen and antibody is insufficient (Hou et al., 2014a; Lisdat and Schafer, 2008). Hence, in order to achieve highly efficient and sensitive impedimetric immunoassay, a series of effective signal amplification approaches have been developed. (1) Using conductive support to immobilize the recognition element has been applied for enhancing the impedance response (Krittayavathananon and Sawangphruk, 2017; Pejcic and Marco, 2006), for the conductivity of the interface can be strongly affected by the antigen-antibody specific

* Corresponding author.
** Corresponding author.
E-mail addresses: mazhanfang@cnu.edu.cn (Z. Ma), hanhongliang@cnu.edu.cn (H. Han).
[1] These authors equally contributed to this work.

https://doi.org/10.1016/j.bios.2019.04.049
Received 15 December 2018; Received in revised form 13 March 2019; Accepted 24 April 2019
Available online 29 April 2019
0956-5663/

recognition (Park and Park, 2009). (2) Binding electronegative material to recognition surface is another amplification path for impedimetric immunosensor (Gao et al., 2018; Park and Park, 2009), which can drastically hinder the charge transfer because of the electrostatic repulsion between redox species $[Fe(CN)_6]^{3-/4-}$ and electronegative material. Despite great progress in signal amplification, the use of negatively charged material can suffer from a relatively minor impedance change in trace concentration of target, which is caused by high initial resistance due to electrostatic repulsion between redox mediator $[Fe(CN)_6]^{3-/4-}$ and electronegative material on electrode surface. (3) Enzyme-catalyzed precipitation techniques have been considered as an efficient approach to increase resistance signal (Hou et al., 2014b; Xie et al., 2018). In this approach, with the help of H_2O_2, enzyme catalyzes the oxidation of substrate to produce nonconductive precipitation on the electrode, which can remarkably amplify the resistance signal by hindering the charge transfer of $[Fe(CN)_6]^{3-/4-}$. However, H_2O_2 is instability and easily decomposes in air, leading to non-specific response (Wu et al., 2015). Meanwhile, time-consuming label functionalization and complex modification process restrict its widespread application. Therefore, to overcome these restrictions, it is still urgent to exploit new efficient methods for signal amplification. Benefited from the advantages of high sensitivity and stability (Berron et al., 2011; Gormley et al., 2014), radical polymerization can be regarded as a promising candidate for signal amplification in the construction of sensing platform. To the best of our knowledge, utilizing cascade catalysis-initiated radical polymerization to impedimetric immunosensor for signal amplification has not been reported.

Herein, copper-based metal-organic framework (Cu-MOF) conjugated with glucose oxidase (GOx) and CA15-3 antibody (Ab_2) was used as immunoprobes, which can not only recognize CA15-3, but also initiate radical polymerization via cascade catalytic reaction. Based on the unique property of the immunoprobes, a new signal amplification approach was proposed to design an impedimetric biosensor for ultrasensitive detection of CA15-3. Upon introduction of immunoprobes, GOx catalyzed glucose oxidation to produce hydrogen peroxide (H_2O_2), while H_2O_2 is subsequently catalyzed by Cu-MOF to react with acetylacetone (ACAC) and result in ACAC radicals for the in-situ formation of poly (N-isopropylacrylamide) (PNIPAM) on the substrate. Due to the poor conductivity, the formed PNIPAM dramatically hindered the charge transfer of $[Fe(CN)_6]^{3-/4-}$ and the resistance difference was elevated prominently. Consequently, the proposed impedimetric immunosensor exhibited ultralow detection limit and wide detection range for ultrasensitive detection of CA15-3, indicating the great potential of this new sensing platform for tumor markers in practical clinical diagnosis.

2. Experimental section

2.1. Materials and reagents

Carbohydrate antigen 15–3 (CA15-3), carbohydrate antigen 19–9 (CA19-9), carbohydrate antigen 12–5 (CA12-5), carbohydrate antigen 24–2 (CA24-2), carcinoembryonic antigen (CEA) and CA15-3 antibody (Ab_1, Ab_2) were purchased from Shanghai Linc-Bio Science Co. Ltd (Shanghai, China). Human serum was provided by Beijing GENIA Biotechnology Co. Ltd. (Beijing, China). Copper nitrate-trihydrate ($Cu(NO_3)_2{\cdot}3H_2O$), $K_4Fe(CN)_6$ and $K_3Fe(CN)_6$ were obtained from Sinopharm Chemical Reagent Co., Ltd (Shanghai, China). 2-amino terephthalic acid ($NH_2{-}H_2BDC$), $HAuCl_4{\cdot}3H_2O$ and KCl were provided by Alfa Aesar (Tianjin, China). Glucose oxidase (GOx), polyvinylpyrrolidone (PVP) and glutaraldehyde (GA) were obtained from Sigma-aldrich (Beijing, China). N-isopropylacrylamide (NIPAM) was obtained from Shanghai Macklin Biochemical Co., Ltd (Shanghai, China). N,N′-methylene-bis-acrylamide (MBA) was provided by Aladdin Chemistry Co., Ltd (Shanghai, China). All solutions were prepared with ultrapure water.

2.2. Apparatus

Electrochemical measurements including electrochemical impedance spectroscopy (EIS) and cyclic voltammetry (CV) were carried out on a three electrode system with multichannel potentiostat (VMP3, France). A conventional three-electrode system in experiment was made up of a modified glassy carbon electrode (GCE, Φ = 4 mm), a platinum wire and a saturated Ag/AgCl electrode as working electrode, counter electrode and reference electrode, respectively. Transmission electron microscope (TEM) image was recorded on a Hitachi (H7650, 80 kV) TEM (Hitachi, Japan). Scanning electron microscope (SEM) was performed on a Hitachi S-4800 SEM (Hitachi, Japan). X-ray photoelectron spectroscopy (XPS) was determined on an Escalab 250 X-ray photoelectron spectroscope (Thermofisher, American). Fourier transform infrared (FTIR) spectra were obtained with a VECTORTM 22 spectrometer (Bruker, Germany). Ultraviolet–visible (UV–vis) spectroscopy measurement was recorded on a UV-2550 UV–vis spectrophotometer (Shimadzu, Japan). Deionized water was used in all processes by PSDK-20-E (Beijing, China).

2.3. Synthesis of Cu-MOF

Cu-MOF nanoparticles were prepared on the basis of published literature with minor modification (Wang et al., 2017). Solution A: 0.2 g PVP was dissolved into the mixed solvent of 4 mL ethanol and 4 mL DMF. Solution B: 5.43 mg $NH_2{-}H_2BDC$ and 24.2 mg $Cu(NO_3)_2{\cdot}3H_2O$ were dissolved into 4 mL ethanol. Then, solution A and solution B were mixed together. After ultrasound 20 min, the mixed solution was transferred into a Teflon-lined autoclave and kept for 6 h at 130 °C. Subsequently, the obtained product was thoroughly washed with ethanol and deionized water. Finally, the collected product was redispersed as solution for further use.

2.4. Synthesis of Ab_2-functionalized GOx-Cu-MOF immunoprobes

Firstly, 2 mL 2.5 wt% glutaraldehyde was added into 2 mL as-prepared Cu-MOF nanoparticles and stirred for 3 h to initiate the reaction. Then, the obtained product was centrifuged (8000 rpm), washed with deionized water repeatedly and re-dispersed in 1 mL deionized water. Afterwards, the mixture containing 100 μL, 1 mg/mL CA15-3 antibody (Ab_2) and 1 mL 6 mg/mL GOx was added and incubated overnight. After that, the mixture was blocked with 1 mL 1.0 wt% BSA for 1 h to avoid the nonspecific absorption. Finally, the immunoprobes were obtained by centrifugation (4000 rpm) and washing, then redispersed as solution and stored at 4 °C.

2.5. Fabrication of the impedimetric immunosensor

Bare glassy carbon electrode (GCE) was repeatedly polished with alumina powders (0.05 μm), which was washed by ultrasound in ethanol and ultrapure water three times. Then, the AuNPs was obtained on GCE by electrodeposition in 1 mM $HAuCl_4$ containing 0.1 M KCl for 30 s under a potential of −0.2 V. After that, 80 μL 200 μg/mL CA15-3 antibody (Ab_1) was incubated on electrode surface at 4 °C overnight (Wang and Ma, 2017). To avoid non-specific binding sites, 20 μL 2 wt% BSA blocking agent was dripped on Ab_1/Au/GCE and incubated for 1 h at room temperature. After every step, the modified electrodes were washed with ultrapure water carefully.

2.6. Electrochemical detection of CA15-3

A series of standard solutions of CA15-3 antigen were incubated on Ab_1-BSA/Au/GCE at 37 °C for 1 h and then washed with deionized water. After that, 20 μL as-prepared immunoprobes were incubated on CA15-3/Ab_1-BSA/Au/GCE at 37 °C for 55 min and then washed carefully to remove unbound probes. Subsequently, the solution (20 μL,

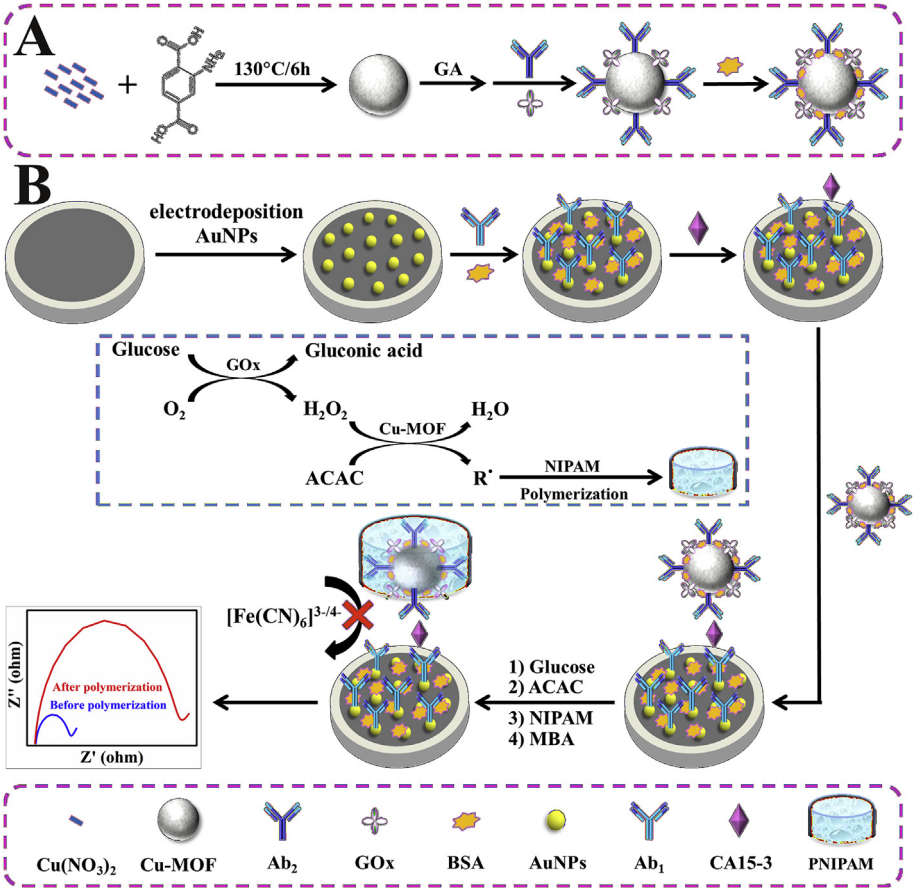

Scheme 1. Preparation process of immunoprobes (A) and schematic illustration of cascade catalysis-initiated radical polymerization triggered signal amplification for electrochemical detection of CA15-3 (B).

containing 0.1 M glucose, 0.4 mM ACAC, 0.25 M NIPAM and 2.5 mM MBA) was dropped on the modified electrodes at room temperature for 40 min to initiate radical polymerization. Then, the electrochemical signals were determined by EIS, which was carried out in 5 mM $[Fe(CN)_6]^{3-/4-}$ containing 0.1 M KCl. In addition, EIS signals were measured at the alternative voltage amplitude of 10 mV, the frequency from 0.02 to 10^5 Hz and the potential of 0 V relative to open circuit voltage.

3. Results and discussion

3.1. Characterization of Cu-MOF and Ab_2-GOx-Cu-MOF

The detailed preparation process of Cu-MOF and Ab_2-GOx-Cu-MOF was shown in Scheme 1A. The morphologies of Cu-MOF nanoparticles were characterized by TEM (Fig. 1A), showing the uniform distribution and the average diameter about 200 nm. The FTIR spectra of NH_2—H_2BDC and Cu-MOF were shown in Fig. 1B. The functional groups of NH_2—H_2BDC contained —COOH and $-NH_2$ (curve a). The characteristic stretching peaks at 1626, 3394 and 3509 cm^{-1} were attributed to the amino group (Karabacak et al., 2010; Sienkiewicz-Gromiuk et al., 2012; Wang et al., 2017; Zhao et al., 2014; Zhou et al., 2017). Meanwhile, the peaks at 1593 and 1690 cm^{-1} were assigned to stretching vibration of C=O and 2992 cm^{-1} was resulted from —OH in —COOH. Owing to the coordination interaction between Cu^{2+} and —COOH of NH_2—H_2BDC, the stretching peak of —OH at 2992 cm^{-1} disappeared (curve b), indicating the formation of Cu-MOF (Wang et al., 2017; Zhou et al., 2017). In addition, the elements of Cu-MOF were illustrated by XPS (Fig. S1). The characteristic peaks at 284.79 eV, 399.74 eV, 532.04 eV and 936.1 eV were attributed to C1s, N1s, O1s and Cu2p, respectively, which were good consistent with the reported literature (Xie et al., 2015; Yao et al., 2015; Zhou et al., 2017). UV–vis spectra of Cu-MOF and Ab_2-GOx-Cu-MOF were shown in Fig. S2. In the presence of H_2O_2 and TMB, the intense peak at 650 nm (Fig. S2A) manifested that Cu-MOF nanoparticles were effective peroxidase mimics. In the presence of glucose and TMB, the absorption peak was observed at 650 nm (Fig. S2B), indicating the successful modification of GOx and the cascade catalysis performance of immunoprobes (Ab_2-GOx-Cu-MOF). As shown in Fig. S3, the mixed solution (0.1 M glucose, 0.4 mM ACAC, 0.25 M NIPAM and 2.5 mM MBA) transformed to polymers with Ab_2-GOx-Cu-MOF by cascade catalysis-initiated radical polymerization, further confirming that GOx was successfully linked to Cu-MOF nanoparticles. All the above observations verified the successful preparation of Cu-MOF and Ab_2-GOx-Cu-MOF.

3.2. Principle of designed impedimetric biosensor

The stepwise modification and determination process of impedimetric immunosensor were illustrated in Scheme 1B. The AuNPs modified layer was electrodeposited on GCE as the matrix of biosensor, which was utilized to improve the interfacial conductivity and immobilize Ab_1 (Zhao and Ma, 2017; Zhao et al., 2019). To avoid nonspecific binding sites, BSA was used as blocking agent. Benefited from high resistance and superior catalytic activity of Cu-MOF, Ab_2 and GOx were covalently conjugated with Cu-MOF by aldehyde functional group of glutaraldehyde as immunoprobes. When the target CA15-3 existed, immunoprobes were specifically captured on the electrode via antibody-antigen specific reaction (BSA-Ab_2-GOx-Cu-MOF/CA15-3/Ab_1-BSA/Au/GCE). With the solution containing glucose, ACAC, NIPAM and MBA dropping on the modified electrodes, the cascade catalysis-initiated radical polymerization was triggered by immunoprobes.

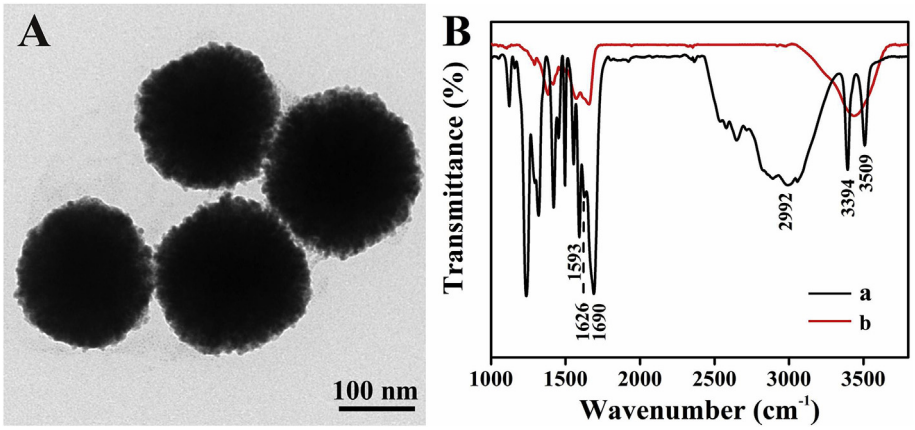

Fig. 1. TEM image of Cu-MOF (A) and FTIR spectra (B) of NH_2—H_2BDC (a), Cu-MOF (b).

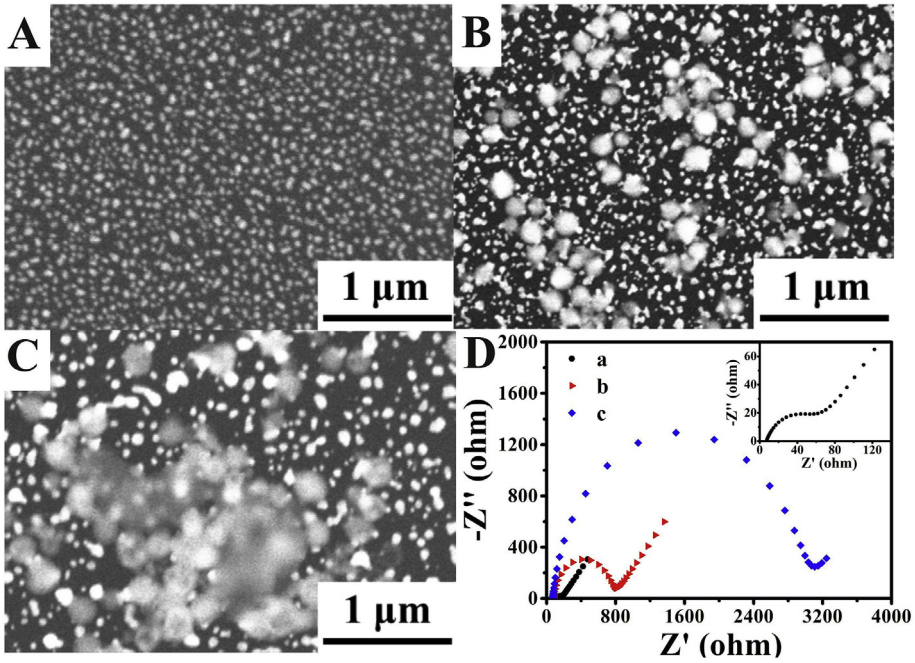

Fig. 2. SEM images of Au/GCE (A), the biosensor incubated with 1 U/mL CA15-3 and immunoprobes before (B) and after (C) radical polymerization. EIS (D) of Au/GCE (a), the biosensor incubated with 1 U/mL CA15-3 and immunoprobes before (b) and after (c) radical polymerization. Inset: Magnified view of EIS of Au/GCE (a).

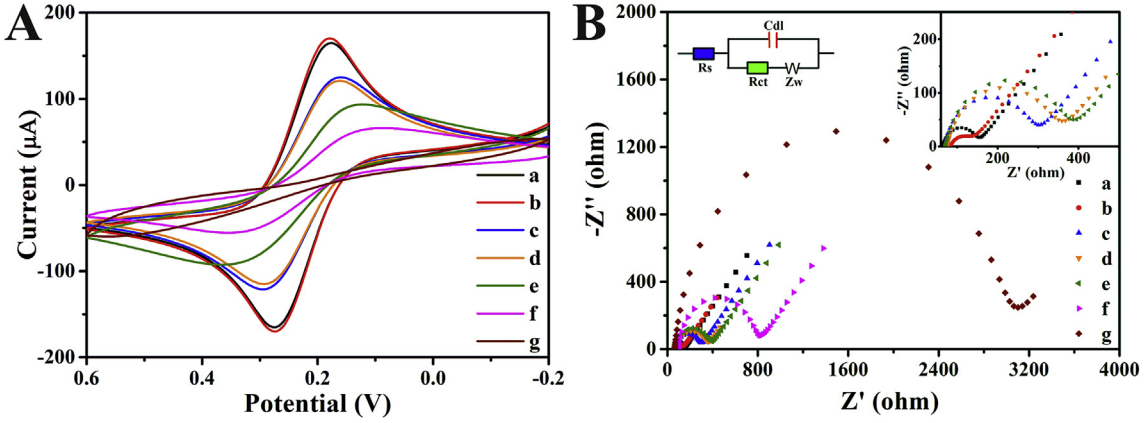

Fig. 3. CV (A) and EIS (B) of different modified electrodes in 5 mM $[Fe(CN)_6]^{3-/4-}$ containing 0.1 M KCl: bare GCE (a), Au/GCE (b), Ab_1/Au/GCE (c), BSA/Ab_1/Au/GCE (d), CA15-3/BSA/Ab_1/Au/GCE (e), BSA-Ab_2-GOx-Cu-MOF/CA15-3/BSA/Ab_1/Au/GCE (f) and signal amplification by radical polymerization (g). Inset: Magnified view of EIS of bare GCE (a), Au/GCE (b), Ab_1/Au/GCE (c), BSA/Ab_1/Au/GCE (d) and CA15-3/BSA/Ab_1/Au/GCE (e).

Firstly, GOx catalyzed the oxidation of glucose, accompanying with the consumption of oxygen and the in-suit formation of H_2O_2. Subsequently, with mimicking peroxidase activity, Cu-MOF catalyzed the reaction between H_2O_2 and ACAC to generate ACAC radicals, which can be utilized for initiating polymerization of NIPAM to form PNIPAM. Furthermore, we used SEM to characterize the morphology of electrode surface in intermediate steps. Seen from Fig. 2A, AuNPs modified by electrodeposition were dispersed uniformly on GCE. After incubation of the immunoprobes, nanocomposites appeared on electrode surface (Fig. 2B) whose size was close to Cu-MOF in Fig. 1A. Translucent substances can be observed in Fig. 2C after dropping the mixed solution (glucose, ACAC, NIPAM and MBA), which can be inferred the formation of polymer (PNIPAM). To further verify the electrochemical processes of electrode surface, the remarkable resistance increase can be observed by EIS measurements (Fig. 2D) on account of the poor conductivity of Cu-MOF and PNIPAM. Therefore, benefited from the polymerization-based signal amplification strategy, the designed impedimetric immunosensor has great potential for ultrasensitive detection of CA15-3.

3.3. Electrochemical characterization of immunosensor

To characterize the stepwise fabrication process of this immunosensor, CV measurement (Fig. 3A) was carried out in 5 mM $[Fe(CN)_6]^{3-/4-}$ containing 0.1 M KCl. Compared with bare GCE (curve a), the AuNPs modified GCE (curve b) showed higher current signal due to high conductivity and large specific surface. After incubation with Ab_1, BSA and CA15-3 antigen (curve c-e), the current signal decreased successively. On account of poor conductivity of immunoprobes (curve f) and polymers (curve g), the current signal further decreased after cascade catalysis-initiated radical polymerization which hindered the electron transfer.

EIS was also measured to monitor the interfacial properties of various modification steps in 5 mM $[Fe(CN)_6]^{3-/4-}$ containing 0.1 M KCl. In Nyquist plots in Fig. 3B, the charge transfer resistance (R_{ct}) was equal to semicircle diameter. The R_{ct} values varied when different substances were modified on the electrodes. Seen from Fig. 3B, after electrodeposition of AuNPs, Au/GCE (curve b) presented a smaller semicircle than the bare GCE (curve a) on account of the enhancement of interfacial conductivity. The impedance increased gradually after immobilization with Ab_1, BSA and CA15-3 antigen (curve c-e). After the capture of immunoprobes (curve f) and the formation of polymers (curve g), resistance values were further increased. The results of EIS were in consistence with CV measurement, indicating the successful fabrication of the designed biosensor.

3.4. Optimization of experimental conditions

In order to obtain the optimum analytical performance, the experimental conditions were optimized, including the incubation time of immunoprobes and the reaction time of radical polymerization. As shown in Fig. S4A, R_{ct} values increased gradually with the incubation time of immunoprobes from 25 to 55 min and reached a plateau after 55 min, indicating the saturated binding between CA15-3 and immunoprobes. Thus, 55 min was chosen as the optimal incubation time of immunoprobes. Also, reaction time of radical polymerization was optimized (Fig. S4B). R_{ct} values can be observed a gradual increase with the time from 10 to 40 min and kept stable after 40 min. Hence, 40 min was selected as optimal reaction time to initiate radical polymerization.

3.5. Signal amplification based on cascade catalysis-initiated radical polymerization

To verify the feasibility of this strategy, the signal amplification of cascade catalysis-initiated radical polymerization on the R_{ct} values was investigated under the optimum experimental conditions. Seen from Fig. 4A, the modified electrodes (Ab_1-BSA/Au/GCE) were incubated without (curve a) and with (curve b) 1 U/mL CA15-3 antigen to show the ΔR_{ct} value ($\Delta R_{ct} = R_{ct2} - R_{ct1}$, where R_{ct1} and R_{ct2} are the R_{ct} value of the immunosensor incubated without and with CA15-3 antigen, respectively) by antigen-antibody specific recognition. According to literature reports (Berron et al., 2011), in fluorescence analysis, since radicals generated by enzymes can trigger a large number of polymerization reactions, signal amplification of polymerization substrate exhibited over three times greater than traditional enzymatic substrate. In order to substantiate the signal amplification effect of polymerization in designed immunosensor, radical polymerization was initiated by cascade catalytic reaction on the modified electrodes (Ab_1-BSA/Au/GCE) which were incubated without (curve a) and with (curve b) 1 U/mL CA15-3 antigen (Fig. 4B). Seen from Fig. 4, the ΔR_{ct} value after radical polymerization (ΔR_{ct2} = 2292.9 Ω) exhibited over seven times greater than that of before radical polymerization (ΔR_{ct1} = 302.3 Ω), indicating that radical polymerization can strengthen the hindrance of charge transfer and amplify the resistance values prominently.

3.6. Analytical performance of immunosensor

Under optimum experimental conditions, R_{ct} values of designed impedimetric biosensor were measured in buffer solution spiked with different CA15-3 antigen (Fig. 5A). The calibration curve exhibited wide linear ranges of two concentration ranges from 0.00001 to 0.01 U/mL and 0.01–100 U/mL, respectively (Fig. 5B, ■). The corresponding calibration regression equations were R_{ct1} = 236.58 lgC + 1923.15 (R_1^2 = 0.9981) for lower concentration range and R_{ct2} = 731.11 lgC + 2920.13 (R_2^2 = 0.9987) for higher concentration range. The ultralow detection limit was 5.06 μU/mL calculated by three times standard deviation of the blank. The assay was also employed to detect CA15-3 in human serum. As shown in Fig. 5B (●), the linear relationship can be obtained in ranges from 0.0001 to 0.01 U/mL and 0.01–100 U/mL. The corresponding linear regression equations were R_{ct1} = 318.35 lgC + 2319.16 (R_1^2 = 0.9968) for lower concentration range and R_{ct2} = 805.24 lgC + 3231.00 (R_2^2 = 0.9949) for higher concentration range, indicating the similar dynamic ranges and calibration regression equations in buffer solution and real serum. In human serum, the detection limit was 19.34 μU/mL, which was slightly higher than that of in buffer solution. Compared with the methods for detection of CA15-3 in recent literature, the immunosensor exhibited higher analytical performance including lower detection limit and wider detection range (Table S1).

3.7. Specificity, reproducibility and stability of immunosensor

To evaluate the specificity of the designed immunosensor for CA15-3 detection, the immunosensor was incubated with several interferences such as CA12-5 (100 U/mL), CA19-9 (100 U/mL), CA24-2 (100 U/mL) and CEA (100 ng/mL). As indicated from Fig. S5, the R_{ct} values caused by interferences can be negligible compared with CA15-3 (1 U/mL). Furthermore, it was found that the R_{ct} value of the mixture containing CA15-3 and the above interferences was almost consistent with that of only CA15-3. These results indicated the designed biosensor exhibited superior selectivity for CA15-3. Moreover, the reproducibility of biosensor was also investigated by testing the R_{ct} value of five modified electrodes. The relative standard deviation (RSD) was 1.66%, suggesting the reproducibility is acceptable. Furthermore, the modified electrodes were stored at 4 °C for three weeks to analyze the stability of biosensor. The R_{ct} values still retained 96.5%, 94.0% and 90.3% of initial value after one week, two weeks and three weeks. In addition, the RSD was 3.18%, 2.86% and 2.67% respectively, indicating the good stability of immunosensor.

3.8. Detection of CA15-3 in real samples

To verify the practical applicability of the designed biosensor, the

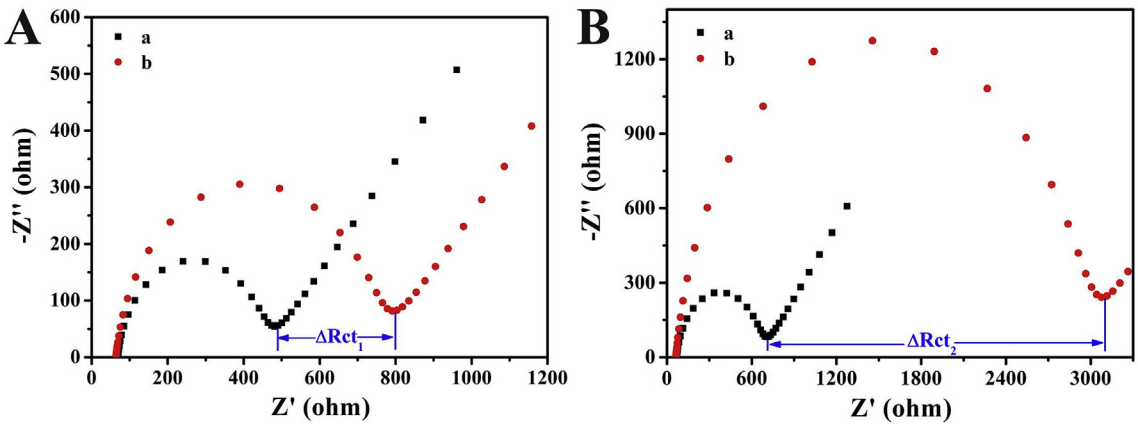

Fig. 4. The contrast of EIS resistance value differences in 5 mM $[Fe(CN)_6]^{3-/4-}$ containing 0.1 M KCl: the immunosensor without (A) and with (B) radical polymerization amplification. The immunosensor was incubated without 1 U/mL CA15-3 (a) and with CA15-3 (b).

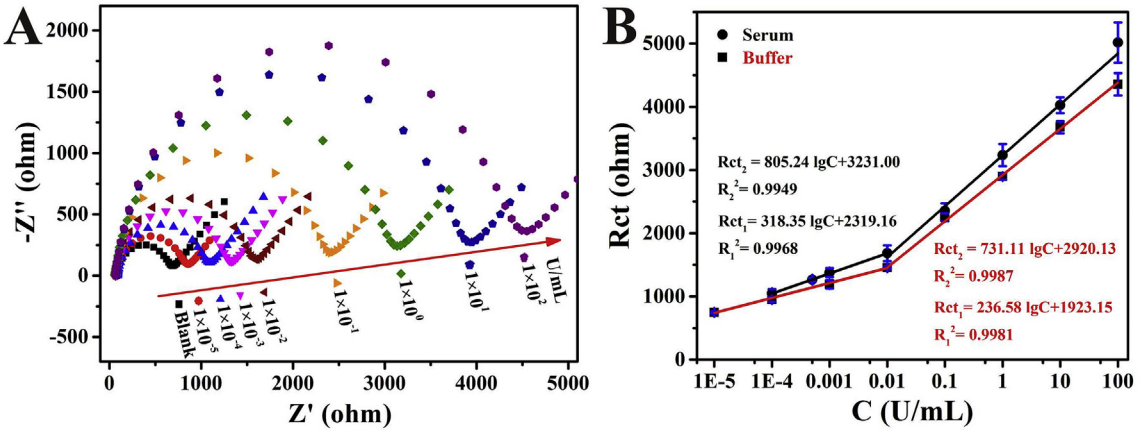

Fig. 5. (A) EIS response of electrochemical biosensor for target CA15-3 from blank to 100 U/mL in buffer solution. (B) The calibration curve of resistance values vs. the concentrations of CA15-3 in buffer solution (■) and human serum (●).

comparison experiments in real samples were tested by chemiluminescence immunoassay analyzer (CMIA) and impedimetric immunosensor. Seen from Table S2, the acceptable RSD (ranging from 1.88% to 2.32%) and relative error (ranging from −9.71% to 3.33%) indicated the promising potential application of designed impedimetric immunosensor in clinical samples.

4. Conclusion

In summary, the Ab_2-functionalized GOx-Cu-MOF immunoprobes can not only recognize CA15-3, but also trigger cascade catalysis to initiate radical polymerization for signal amplification. A new electrochemical sensing platform based on cascade catalysis-initiated radical polymerization was designed to construct an impedimetric immunosensor for ultrasensitive detection of CA15-3. Noteworthy, the ΔR_{ct} value caused by target after polymerization-based amplification exhibited over seven times greater than that before polymerization, indicating the remarkable effect of signal amplification. Thus, given its excellent analytical performance of the designed impedimetric immunosensor, this ultrasensitive detection platform provided the promising possibility for a broad range of tumor markers.

CRediT authorship contribution statement

Chi Zhang: Data curation, Formal analysis, Investigation, Methodology, Software, Visualization, Writing - original draft. **Dongsheng Zhang:** Data curation, Formal analysis, Investigation, Methodology, Software, Visualization, Writing - original draft. **Zhanfang Ma:** Funding acquisition, Project administration, Resources, Supervision, Validation, Writing - review & editing. **Hongliang Han:** Funding acquisition, Project administration, Resources, Supervision, Validation, Writing - review & editing.

Acknowledgements

High-level Teachers in Beijing Municipal Universities in the Period of 13th Five-year Plan (IDHT20180517) with Capacity Building for Sci-Tech Innovation - Fundamental Scientific Research Funds (025185305000/195).

Appendix A. Supplementary data

Supplementary data related to this article can be found at https://doi.org/10.1016/j.bios.2019.04.049.

References

Akbari Nakhjavani, S., Khalilzadeh, B., Samadi Pakchin, P., Saber, R., Ghahremani, M.H., Omidi, Y., 2018. Biosens. Bioelectron. 122, 8–15.
Berron, B.J., Johnson, L.M., Ba, X., McCall, J.D., Alvey, N.J., Anseth, K.S., Bowman, C.N.,

2011. Biotechnol. Bioeng. 108, 1521–1528.
de Oliveira, R.A.G., Materon, E.M., Melendez, M.E., Carvalho, A.L., Faria, R.C., 2017. ACS Appl. Mater. Interfaces 9, 27433–27440.
DeSantis, C., Naishadham, D., Jemal, A., 2013. CA A Cancer J. Clin. 63, 151–166.
Gao, F., Zhang, T., Chu, Y., Wang, Q., Song, J., Qiu, W., Lin, Z., 2018. Microchim. Acta 185, 555.
Gormley, A.J., Chapman, R., Stevens, M.M., 2014. Nano Lett. 14, 6368–6373.
Hashemi, P., Afkhami, A., Bagheri, H., Amidi, S., Madrakian, T., 2017. Anal. Chim. Acta 984, 185–192.
Hou, L., Gao, Z., Xu, M., Cao, X., Wu, X., Chen, G., Tang, D., 2014a. Biosens. Bioelectron. 54, 365–371.
Hou, L., Tang, Y., Xu, M., Gao, Z., Tang, D., 2014b. Anal. Chem. 86, 8352–8358.
Jemal, A., Bray, F., Center, M.M., Ferlay, J., Ward, E., Forman, D., 2011. CA A Cancer J. Clin. 61, 69–90.
Jiang, X., Wang, H., Yuan, R., Chai, Y., 2015. Biosens. Bioelectron. 63, 33–38.
Karabacak, M., Cinar, M., Unal, Z., Kurt, M., 2010. J. Mol. Struct. 982, 22–27.
Ke, H., Zhang, X., Huang, C., Jia, N., 2018. Biosens. Bioelectron. 103, 62–68.
Krittayavathananon, A., Sawangphruk, M., 2017. Anal. Chem. 89, 13283–13289.
Li, H., He, J., Li, S., Turner, A.P.F., 2013a. Biosens. Bioelectron. 43, 25–29.
Li, X., Li, Y., Feng, R., Wu, D., Zhang, Y., Li, H., Du, B., Wei, Q., 2013b. Sens. Actuators, B 188, 462–468.
Lisdat, F., Schafer, D., 2008. Anal. Bioanal. Chem. 391, 1555–1567.
Marques, R.C.B., Costa-Rama, E., Viswanathan, S., Nouws, H.P.A., Costa-García, A., Delerue-Matos, C., González-García, M.B., 2018. Sens. Actuators, B 255, 918–925.
Park, J.Y., Park, S.M., 2009. Sensors 9, 9513–9532.
Pejcic, B., Marco, R.D., 2006. Electrochim. Acta 51, 6217–6229.
Ren, X., Ma, H., Zhang, T., Zhang, Y., Yan, T., Du, B., Wei, Q., 2017. ACS Appl. Mater. Interfaces 9, 37637–37644.
Sharma, S., Zapatero-Rodríguez, J., Saxena, R., O'Kennedy, R., Srivastava, S., 2018. Biosens. Bioelectron. 106, 78–85.
Sienkiewicz-Gromiuk, J., Mazur, L., Bartyzel, A., Rzączyńska, Z., 2012. J. Inorg. Organomet. Polym. Mater. 22, 1325–1331.
Tang, Z.X., Wang, L.Y., Ma, Z.F., 2017. Biosens. Bioelectron. 92, 577–582.
Wang, H.Q., Ma, Z.F., 2017. Microchim. Acta 184, 1045–1050.
Wang, S., Deng, W., Yang, L., Tan, Y., Xie, Q., Yao, S., 2017. ACS Appl. Mater. Interfaces 9, 24440–24445.
Wu, Q., Wang, X., Liao, C., Wei, Q., Wang, Q., 2015. Nanoscale 7, 16578–16582.
Xie, S., Tang, Y., Tang, D., Cai, Y., 2018. Anal. Chim. Acta 1023, 22–28.
Xie, S., Ye, J., Yuan, Y., Chai, Y., Yuan, R., 2015. Nanoscale 7, 18232–18238.
Xu, Y., Cheng, G., He, P., Fang, Y., 2009. Electroanalysis 21, 1251–1259.
Yao, W., Li, F.-L., Li, H.-X., Lang, J.-P., 2015. J. Mater. Chem. 3, 4578–4585.
Zhang, D.S., Li, W.X., Ma, Z.F., 2018a. Biosens. Bioelectron. 109, 171–176.
Zhang, K., Lv, S., Lu, M., Tang, D., 2018b. Biosens. Bioelectron. 117, 590–596.
Zhang, L., He, Y., Wang, H., Yuan, Y., Yuan, R., Chai, Y., 2015. Biosens. Bioelectron. 74, 924–930.
Zhang, X., Peng, X., Jin, W., 2006. Anal. Chim. Acta 558, 110–114.
Zhao, L.H., Ma, Z.F., 2017. Sens. Actuators, B 241, 849–854.
Zhao, L.H., Yin, S., Ma, Z.F., 2019. ACS Sens. 4, 450–455.
Zhao, M., Deng, K., He, L., Liu, Y., Li, G., Zhao, H., Tang, Z., 2014. J. Am. Chem. Soc. 136, 1738–1741.
Zheng, Y., Zhao, L.H., Ma, Z.F., 2018. Biosens. Bioelectron. 115, 30–36.
Zhou, X., Guo, S., Gao, J., Zhao, J., Xue, S., Xu, W., 2017. Biosens. Bioelectron. 98, 83–90.